https://doi.org/10.15407/ufm.23.04.583

Yu.G. CHABAK [1,2,*], V.I. ZURNADZHY [1], M.A. GOLINSKYI [1], V.G. EFREMENKO [1,2,], N.P. ZAICHUK [3], I. PETRYSHYNETS [2], and S.P. SHYMCHUK [3,***]**

[1] Pryazovskyi State Technical University,
7 Universytets'ka Str., UA-87555 Mariupol, Ukraine

[2] Institute of Materials Research of Slovak Academy of Sciences,
47 Watsonova Str., SL-04001 Kosice, Slovakia

[3] Lutsk National Technical University,
75 Lvivs'ka Str., UA-43018 Lutsk, Ukraine

* julia.chabak25@gmail.com, ** vgefremenko@gmail.com, *** s.shimchuk@lntu.edu.ua

CURRENT FUNCTIONAL MATERIALS FOR WEAR-RESISTANT CASTING: FROM MULTICOMPONENT CAST IRONS TO HYBRID HIGH-BORON ALLOYS

The results obtained in the last two decades in the development of functional tribological alloys for the castings working under severe abrasion, erosion, and erosion–corrosion conditions are reviewed. The chemical composition, microstructural features, mechanical and tribological properties of (a) multicomponent cast irons, (b) Fe–C–B alloys with an increased (1–3.5 wt.%) boron content, and (c) hybrid abrasive-resistant alloys designed by combining different alloying principles are analysed. The necessity for the formation of a heterophase structure consisting of multitype hard compounds (carbides, borides, and carboborides) distributed in a secondary-hardened martensite matrix is highlighted as a key approach to reaching an advanced abrasive wear resistance of the cast components. The target structural state can be obtained by simultaneous adding several strong carbide-forming elements (Ti, W, Mo, V, and Cr) taken in the same amount (by analogy with high-entropy alloys). This allows the elements to compete with each other to form different phases during crystallization, which ensures the general refinement of the alloy

Citation: Yu.G. Chabak, V.I. Zurnadzhy, M.A. Golinskyi, V.G. Efremenko, N.P. Zaichuk, I. Petryshynets, and S.P. Shymchuk, Current Functional Materials for Wear-Resistant Casting: from Multicomponent Cast Irons to Hybrid High-Boron Alloys, *Progress in Physics of Metals*, **23**, No. 4: 583–612 (2022)

structural constituents. The advantages of partial replacement of carbon with boron in Fe-based alloys are emphasised that allows the formation of boride and carboboride compounds having much higher hardness compared to carbides. This makes it possible to achieve an advanced level of wear resistance in the absence (or at low content) of alloying elements, benefiting from a significant reduction in the cost of the alloy. The influence of alloying elements on the physical and mechanical properties of boride phases is analysed; prospects are outlined, and novel ('hybrid') alloys combining the multialloying principle with high boron content are presented. The main technological approaches applied to improve the mechanical and tribological properties of boron-containing wear-resistant casting are described.

Keywords: multicomponent cast iron, high-boron cast iron, wear resistance, microstructure, boron, carbides, borides.

1. Introduction

In recent decades, the problem of wear of machines and mechanisms has become increasingly acute in connection with the constant intensification of technological processes in mining, transport, energy and many other areas of production [1, 2]. According to Ref. [1], in total, circa 23% (119 EJ) of the world's energy consumption is caused by tribological interactions, of which 20% is spent on overcoming friction and 3% on the repair (or replacement) of worn parts and equipment. Therefore, the challenge of increasing the wear resistance of materials by optimizing their chemical composition, structure and properties regarding the specific operating conditions is becoming more relevant.

Abrasive wear is one of the most common mechanisms of surface destruction in various technological processes, which leads to significant economic losses and has a significant impact on global energy consumption and greenhouse gas emissions. The phenomenon of abrasive wear is associated with the interaction of the working surface with the sliding hard particles being under the normal load [3]. The mechanism and intensity of abrasive wear are generally determined by the 'surface hardness/particle hardness' ratio, that is, hardness is one of the most important criteria for the abrasive resistance of a material. Another key factor is the character of the microstructure, namely the presence of reinforcing high-hardness compounds (carbides, borides, nitrides) and the properties of the metal matrix of the alloy (toughness, the ability to prevent the spalling of particles, as well as the susceptibility to structural transformations induced by the wear process) [4–6]. The type, size, volume fraction, and morphology of hard inclusions, as well as the properties and metastability of the metal matrix should be adapted to specific wear conditions [1].

Over the last century, abrasion-resistant metallic materials have undergone a process of evolution from Hadfield high-manganese steel and unalloyed chilled cast iron to modern abrasion-resistant alloys, which

include high-alloyed white cast irons, high-speed steels (HSSs), high-entropy alloys (HEAs), cold-formed die steels, cemented carbide alloys, particle-reinforced metal matrix composites (PMMCs), *etc.* [7–10]. A wide range of conventional and innovative technologies are focused to modify a working surface via structural and chemical modification as well as coating deposition to create protecting layers of up to several millimetres thick [11–13]. However, in many applications, the wear-induced volume loss is much bigger; thus, the parts should be manufactured from special materials ensuring higher bulk wear resistance. The increased requirements for wear-resistant materials imply using non-standard solutions when creating new types of tribological alloys.

2. Multicomponent Cast Irons

One of the relatively new classes of wear-resistant alloys is 'multicomponent cast irons' (MCCIs), which were first proposed by Matsubara with co-authors [14, 15] in the mid-1990s to increase the durability of rolls of hot rolling mills. The idea of MCCIs followed the known concept of alloying high-speed steel M2 (ASTM A600), which implies the addition of several carbide-forming elements in approximately equal proportions (M2 steel contains 0.78–0.88 wt.% C, 5.50–6.75 wt.% W, 4.50–5.50 wt.% Mo, 3.75–4.50 wt.% Cr, and 1.75–2.20 wt.% V). A basic chemical composition of MCCI is (in wt.%) Fe–2 C–5 Cr–5 Mo–5 W–5 V–5 Co [16]. Molybdenum and tungsten (which act similarly) are adopted in MCCIs to form complex carbides $(Mo, W, Fe)_2C$ or M_2C, and $(Mo, W, Fe)_6C$ or M_6C, where M denotes a metal (martensite). Being dissolved in matrix, Mo and W improve the hardenability and promote the secondary precipitation hardening under tempering (which is important for hot temperature wear applications). Vanadium forms hard eutectic carbides (V, Fe)C or $(V, Fe)_4C_3$ (denoted as MC); also, it takes part in secondary hardening. Chromium is partially dissolved in matrix inhibiting pearlite and bainite transformations, thus, enhancing the hardenability. In addition, Cr contributes to wear resistance through eutectic carbide M_7C_3, which is harder than cementite carbide. In their turn, carbides M_2C, M_6C, and MC are harder than M_7C_3. Cobalt decreases the hardenability but it greatly improves the high-temperature strength suppressing the heat-induced grain coarsening. Thus, MCCIs feature a multiphase structure consisting of different hard carbides dispersed in the metallic matrix.

The main feature which distinguishes MCCIs from M2-HSS is about two-fold increased carbon content (1.8–2.2 wt.%) [17]. Carbon concentration controls the crystallization path and the set of carbide phases in MCCIs. According to [18], carbon content is selected based on C_{bal}

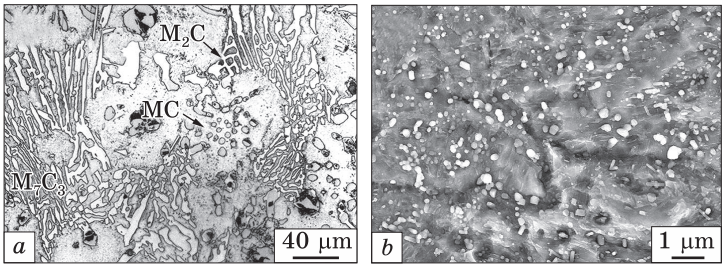

Fig. 1. Microstructure of multicomponent cast iron: (*a*) as-cast state, (*b*) the secondary carbide precipitates (heat-treated state)

calculation:

$$C_{bal} = C - C_{stoich}, \quad (1)$$

where C_{bal} is the carbon fraction dissolved in matrix, C is total carbon content in the alloy (wt.%), C_{stoich} is carbon fraction bound equally with all the carbide-forming elements.

When M_7C_3 carbide is not formed in the alloy upon solidification, C_{stoich} can be found by the Eq. (2) [18]:

$$C_{stoich} = 0.060Cr + 0.063Mo + 0.033W + 0.235V; \quad (2)$$

here, Cr, Mo, W, and V are the concentrations (wt.%) of the Cr, Mo, W, and V, respectively, in the alloy.

If carbide M_7C_3 crystallizes in the alloy, then, Eq. (3) should be applied to calculate C_{stoich} [18]:

$$C_{stoich} = 0.099Cr + 0.063Mo + 0.033W + 0.235V. \quad (3)$$

Different types of carbide can be obtained in MMCI depending on the C_{bal} value. At $C_{bal} \leq 0$, the solidification follows through the transformations (4) [18]:

$$L_0 \rightarrow [(\gamma + MC) + L_1] \rightarrow [L_1 \rightarrow (\gamma + M_2C)], \quad (4)$$

and, at $C_{bal} > 0$, the solidification path is changed to [18]:

$$[L_0 \rightarrow (\gamma + MC) + L_1] \rightarrow [L_1 \rightarrow (\gamma + M_7C_3) + L_2] \rightarrow [L_2 \rightarrow (\gamma + M_2C)], \quad (5)$$

where L_0 is the initial liquid, L_1 and L_2 are the liquids at different stages of solidification. The microstructure for $C_{bal} > 0$ is presented in Fig. 1, *a*.

The crystallization sequence (5) was confirmed by Pasini *et al.* [19] for HEA-inspired multicomponent cast iron of the chemical composition of (in wt.%) 3.45 C, 21.4 Cr, 11.15 Mo, 7.3 V, 6.3 Mn, 0.6 Nb, 2.0 Co. According to the high-entropy alloys' concept, this composition included more than five carbide-forming elements ensuring the configuration entropy at liquid state is greater than $1.5R$, where R is the ideal gas constant.

The authors of Ref. [20] studied MCCIs alloyed by 20 wt.% of carbide-forming elements. They proposed the following solidification sequences depending on chemical composition:

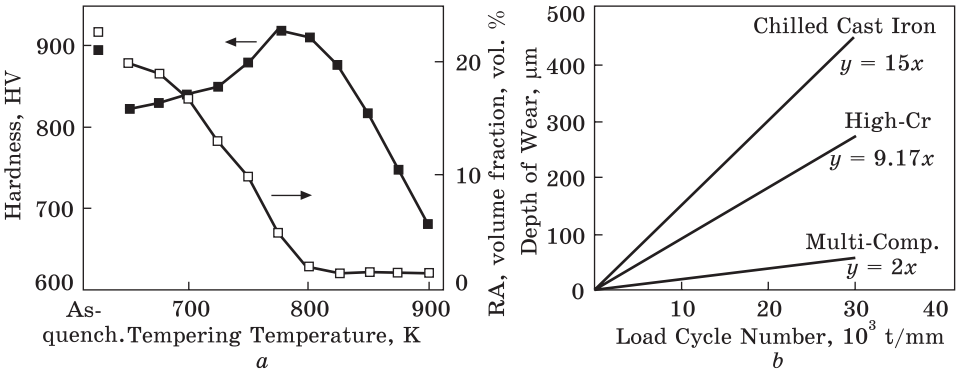

Fig. 2. Heat treatment and wear behaviour of MCCIs: (*a*) effect of tempering temperature on hardness and retained austenite volume fraction, (*b*) wear performance of rolls for hot roll mill. (Constructed based on the results of [18])

for the alloy (in wt.%) Fe–3 C–10 Cr–5 Mo–5 W,

$$[L_0 \rightarrow \text{primary } \gamma + L_1] \rightarrow [L_1 \rightarrow (\gamma + M_7C_3) + L_2] \rightarrow [L_2 \rightarrow (\gamma + M_6C)]; \quad (6)$$

for the alloy (in wt.%) Fe–3 C–10 V–5 Mo–5 W,

$$[L_0 \rightarrow \text{proeutectic } MC + L_1] \rightarrow [L_1 \rightarrow \text{primary } \gamma + L_2] \rightarrow$$
$$\rightarrow [L_2 \rightarrow (\gamma + MC) + L_3] \rightarrow [L_3 \rightarrow \gamma + M_2C]. \quad (7)$$

To address maximally the working conditions specific for the rolling mills, MCCIs should be subjected to heat treatment which is quenching from 1050–1100 °C and tempering at 500–550 °C. Under the austenitization, the secondary carbides MC, M_6C, and M_7C_3 precipitated from austenite [21, 22] (Fig. 1, *b*). Figure 2, *a* illustrates the typical tempering behaviour of MCCI (constructed based on summarizing the results of Matsubara [18]). After quenching, the volume fraction of retained austenite (RA) may reach up to 25 vol.%. During tempering at 500–550 °C, the RA decomposition occurs *via* carbide precipitation (the secondary hardening). Simultaneously, martensite decomposition takes place through the sequent carbide reactions (illustrated for molybdenum as follows [23]):

$$\text{Martensite (Fe, Mo, C)} \rightarrow (\text{Fe, Mo})_3\text{C} \rightarrow (\text{Mo, Fe})_3\text{C} \rightarrow \text{Mo}_6\text{C}. \quad (8)$$

As a result, after the tempering at 500–550 °C, the RA amount sharply decreases while hardness increases to 900–940 HV_{30} [18, 21, 22].

The RA volume fraction in as-quenched MCCIs is increased with austenitization temperature and carbon content [18]. In its turn, the secondary hardening behaviour is controlled by chromium content. The maximum tempered hardness of MCCIs is attributed to 5–7 wt.% Cr; with further Cr content increase, RA stabilizes and the degree of secondary hardening decreases [21]. Inthidech and Matsubara concluded

[23] that the C_{bal} value should be as close to zero to obtain the maximum MCCI hardness after heat treatment.

The formation of a multiphase structure of the composite type (carbides, MC, M_6C, M_2C, M_7C_3 embedded into martensite matrix) ensures an advanced wear resistance of MCCIs. Figure 2, *b* illustrates the wear behaviour (under hot rolling conditions) of MCCI which is roughly 7 times of unalloyed chilled cast irons and 4 times of high-Cr cast iron. Similar results were reported by Wang *et al.* [24] who created a high-entropy microstructure in Fe–20 wt.% Cr–5 wt.% C alloy by adding Ti, V, Mo, and W. It was highlighted that, by adding strong carbide-forming elements, coarse primary M_7C_3 carbides were substituted by finer eutectic carbides M_7C_3, MC, and M_6C leading to promising improvement in the wear resistance of resultant multicomponent cast iron. This remarkable wear behaviour was a ground for the successful application of multicomponent white cast irons in metallurgy (for hot work rolls) and in the cement industry (for the pulverizing mill rolls) [18].

The structure and chemical composition of multicomponent cast irons are in the stage of further improvement [25–28]. Kusumoto *et al.* [27] concluded that the addition of 3 wt.% Ni increases the two-body abrasion resistance of (in wt.%) Fe–2C–5Cr–5Mo–5W–5V–5Co alloys due to more promoted carbide formation by suppressing the solution of the carbide-forming elements in the matrix. The same positive effect of Ni was reported by Zhang *et al.* [25] for MCCI's high-temperature (900 °C) erosion resistance: Ni was explained to enhance the secondary carbide precipitation under austenitization thus strengthening the matrix at elevated temperature. As shown in Ref. [28], an increase in Co content gradually decreases the rate of high-temperature erosion of MCCI since cobalt suppresses the oxidation by forming a protective film of stable spinel-type oxide. In contrast, vanadium accelerates oxidation thus increasing the erosion rate [25]. The hardness of as-quenched MCCI progressively increases when the molybdenum content varies from 0.12 to 7.66 wt.%; however, the best secondary hardening under tempering was attributed to 4.98 wt.% Mo [29].

The idea of 'semi-multicomponent cast iron' was proposed in Ref. [23] to address the needs of centrifugal casting (CF) adopted to produce composite bimetallic mill rolls. In CF-cast rolls, the segregation of eutectic carbides occurs because of the difference in their specific weight. To overcome this problem, the contents of extremely heavy and extremely light carbide-forming elements in the alloy should be controlled. Therefore, MCCIs intended for CF-casting should contain a lower amount of such elements as compared to conventional MCCIs. The authors of Ref. [23] investigated the effect of heat treatment on MCCIs with a content of 'light' chromium varied from 3 to 9 wt.% under the low fixed contents of 'heavy' elements Mo (2 wt.%) and W (1 wt.%). It was found that

semi-MCCIs perform the secondary hardening behaviour close to the basic MCCIs reaching the rather high hardness after 1050 °C quenching and 500 °C tempering (830 HV_{30}) and after 1100 °C quenching and 550 °C tempering (862 HV_{30}). Moreover, the semi-MMCIs provide a more favourable 'properties/costs' balance due to lower alloying by expensive W and Mo.

3. High-Boron Cast Irons

3.1. Boron as a Key Element of Wear-Resistant Alloys

Despite the advanced performance of MCCIs, their wear resistance is limited by the microhardness of the carbides M_6C, M_2C, and M_7C_3, which do not exceed 1800–2000 *HV* [30]. Moreover, MCCIs are rather expensive which is not beneficial for their wide applications. In search of a cheaper and more wear-resistant option, researchers pay more and more attention to boron when developing new alloys. A comparison of the hardness of carbides and borides formed by the same alloying element shows that, as a rule, borides have the highest hardness [30] (see Table). For example, in Fe–C alloys, carbide Fe_3C has a hardness of about 1000 *HV* [31], while the hardness of borocementite $Fe_3(B, C)$ in Fe–C–B ternary alloys is in the range from 1000 to 1600 *HV* [32]. The higher hardness of

Table. **Crystal structure and hardness of carbides and borides [30]**

Element	Carbides		Borides	
	Type, lattice	Hardness, GPa	Type, lattice	Hardness, GPa
Fe	Fe_3C, rhombohedral	8.0–11.0	FeB, orthorhombic Fe_2B, tetragonal	15.0–22.0 18.7
Cr	Cr_7C_3, hexagonal $Cr_{23}C_6$, cubic Cr_3C_2, rhombohedral	13.8 9.7 13.3	Cr_2B, rhombohedral CrB, rhombohedral CrB_2, hexagonal	13.5 21.0 22.0
Mo	Mo_2C, hexagonal	15.0	MoB, tetragonal MoB_2, hexagonal	23.0–24.5 21.3–24.2
W	WC, hexagonal W_2C, hexagonal	21.0 19.9	WB, hexagonal WB_2, hexagonal	— 20.5–22.1
V	$VC_{0.87}$, cubic	29.0	VB_2, hexagonal	28.0
NbC	$NbC_{0.99}$, cubic	24.0	NbB, rhombohedral NbB_2, hexagonal	22.0 26.0
Ti	TiC, cubic	29.0	TiB_2, hexagonal	34.8
Zr	$ZrC_{0.97}$, cubic	26.0	ZrB_2, hexagonal	21.9
Hf	$HfC_{0.99}$, cubic	27.0	HfB_2, hexagonal	29.0
Ta	$TaC_{0.98}$, cubic	25.0	TaB_2, hexagonal	26.0

borocementite is explained by the stronger hybridization of the 'metal–boron' bond, which was established by calculations using the example of cementite-like compounds Fe_3C and Fe_3B [33]. Being added to iron, boron forms borides Fe_2B and FeB, which are about two times harder than Fe_3C. When added to the alloyed cast iron, boron contributes to the formation of alloyed borides MB and M_2B (here, M is a transition metal), the hardness of which, as follows from Table, in most cases, exceeds the hardness of analogous carbides that provides the alloy with a high level of hardness and wear resistance. These properties of boron have long been widely used in surface engineering to create protective layers with increased wear resistance and high-temperature oxidation resistance [34]. An important advantage of boron is its low cost, which makes it possible to create relatively cheap wear-resistant alloys. Considering the prospects of boron-containing alloys, a new generation of wear-resistant materials is currently being developed, in which boron plays a key role [35].

Boron is a chemical element under number 5 in the periodic table, a metalloid belonging to the 13th group of this system. It exists as a simple substance and in the form of compounds, has a high melting point (2076 °C). Boron is a neighbour of carbon in the periodic table, but when added to an alloy it behaves somewhat differently than carbon. In metallurgy, boron is widely used as a microalloying element, which is added in a very small amount (0.0001–0.004 wt.%) to low-carbon structural steel to improve its mechanical properties by inhibiting the pearlitic transformation [36]. At the moment, the effect of boron on the structure and properties of cast iron has been studied quite fully, however, in most works, boron is introduced in small amounts aiming not to the formation of boride phases, but to increase the microhardness of carbides without changing their stoichiometry [37]. Boron affects the eutectic point of white cast iron shifting it to lower carbon content, thus, increasing the volume fraction of carbide precipitates. As shown in Ref. [38], adding 0.5 wt.% B to (in wt.%) 3 C–15 Cr–2 Mo cast iron changed its structure from hypoeutectic to hypereutectic without forming the boride phases. At the same time, boron introduced into Fe–C system alloys in larger quantities can form borides and carboborides, which possess significantly higher hardness and heat resistance as compared with carbides [39].

According to the Fe–B phase diagram (Fig. 3, *a* [40]), the solubility of boron in iron is ≤0.02 wt.% at 1149 °C in austenite and less than 0.0004 wt.% at ≤700 °C in ferrite [41]. This values are extremely low the values compared to the relatively high solubility of carbon in austenite (2.11 wt.% at 1148 °C) and in ferrite (0.0218 wt.% at 727 °C). Guo and co-author [42] found that, in the presence of some alloying elements (Cr, V, Mo), the solubility of boron in α-Fe (martensite) increases to 0.015–0.0589 wt.%. This is explained by the larger atomic

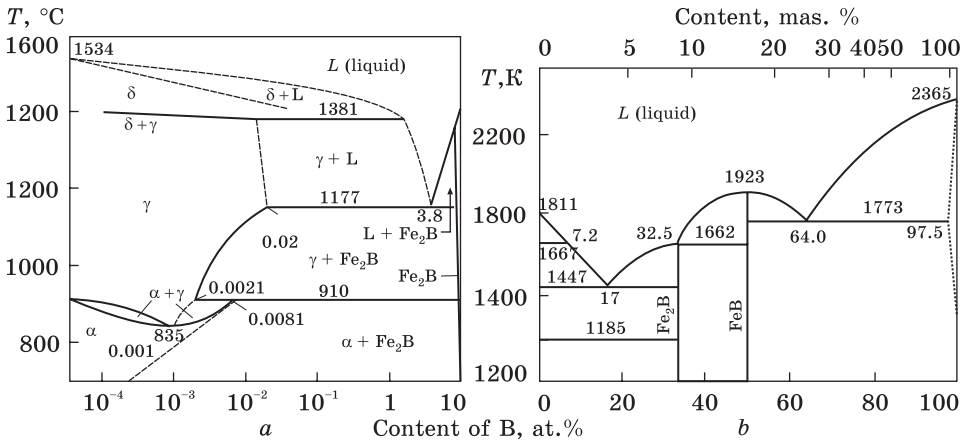

Fig. 3. Phase diagram of Fe–B with (*a*) the low boron content interval [41] and (*b*) full range of boron content [40]

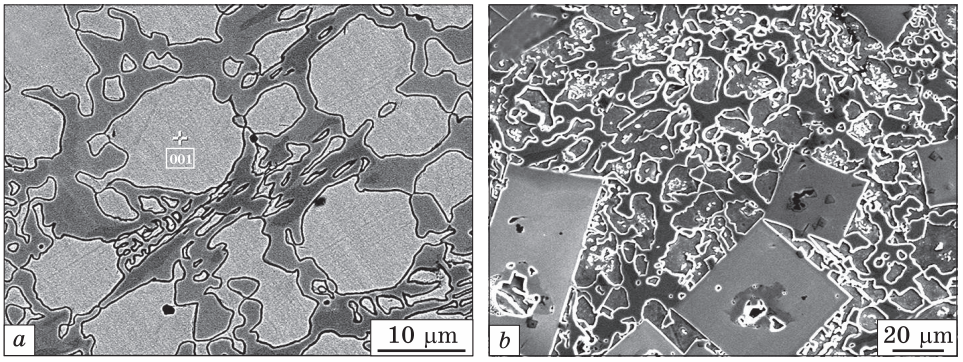

Fig. 4. M_2B-eitectic network (*a*) and (*b*) primary borides M_2B in high-boron alloys

radius of these elements compared to iron, which causes an expansion of the crystal lattice of the α-phase with a corresponding increase in the space for boron atoms accommodation.

If the boron content exceeds its solubility limit, FeB and Fe_2B boride phases are formed (Fig. 3, *b* [41]). Boride Fe_2B contains 33.5 at.% B (8.79 wt.% B). It has a tetragonal lattice *C*16 of space group *I*4/*mcm* (140), type $CuAl_2$, with 12 atoms in a space cell, and the lattice parameters $a = 0.5099$ nm, $c = 0.4240$ nm. In the crystal cell of Fe_2B boride, boron atoms are located at the vertices of a tetragonal prism [43]. Fe_2B crystallizes at 1407 °C according to the peritectic reaction 'L + FeB → Fe_2B'. In alloys containing up to 8.8 wt.% B, Fe_2B boride is formed by the eutectic reaction '$L \rightarrow \gamma + Fe_2B$', which occurs at 1177 °C (1147 °C [41]). The eutectic ($\gamma + Fe_2B$) has the form of a continuous three-dimensional (3*D*) network surrounding austenite dendrites (Fig. 4, *a*).

Boron-rich boride FeB contains 50 at.% B (16.17 wt.% B) with a homogeneity range of about 1 at.%. FeB has an orthorhombic lattice *B*27 of space group *P*/*bnm* with cell parameters $a = 0.4053$ nm, $b = 0.5495$ nm, $c = 0.2946$ nm. FeB boride melts congruently at 1590 °C [44]; its crystal structure is formed by 'zigzag' chains of boron atoms, which coordinate with seven iron atoms in the form of a trigonal prism [45].

Due to better mechanical properties, the Fe_2B phase is considered more acceptable than FeB [46]. The mechanical and thermal properties of Fe_2B boride were studied in detail in works [47, 48]. The modulus of elasticity and hardness of Fe_2B are 331.52 GPa and 19.04 GPa, respectively, and the hardness of Fe_2B exceeds the hardness of a chromium-based carbide M_7C_3 (16.43 GPa) and $Fe_{23}(C, B)_6$ borocarbide (10.39 GPa) [48]. It was established that the hardness of F_2B depends on the direction of indentation relative the crystallographic planes in the boride crystal: its hardness reaches a maximum in the plane perpendicular to the direction of the boride growth [49].

At hypereutectic boron concentration, the primary boride Fe_2B crystallizes in the form of large prismatic inclusions (Fig. 2, *b*), increasing the wear resistance and reducing the fracture toughness of the alloy. The shape of primary borides is controlled by the preferential boride growth in the (001) direction due to the structural anisotropy of the Fe_2B crystal (some crystal planes lack boron atoms [50, 51]). The sizes of primary Fe_2B boride inclusions can be reduced by adding various modifiers to the melt, such as (K + Na) [52] or (Ti + N) [53], which decrease the surface tension at the liquid/boride interface or create crystallization centres with a corresponding increase in the number boride nuclei.

Taking into account the above, the introduction of high boron content into Fe-based alloys is a logical and expedient direction in the development of abrasion-resistant alloys with high abrasion resistance [54]. This direction was firstly formulated by Lakeland *et al.* [55] in the early 2000s. He proposed Fe-based alloys added with high (several percent) boron amounts with a simultaneous decrease in the carbon concentration. The main idea behind such changes was to replace cementite carbide with a harder Fe_2B iron boride, which was supposed to crystallize in the form of a eutectic network with increased wear resistance. The fairly low concentration of carbon is due to the desire to increase the ductility and toughness of the matrix areas: since carbon is mostly concentrated in the matrix, leading to its low toughness; then, carbon content must be limited to prevent sharp embrittlement of the alloy. The volume fraction of borides in Fe–B–C alloys, in turn, is controlled by boron content: with its increase, the hardness of the alloy gradually increases due to the formation of a larger number of borides and carboborides. Proposed by Lakeland, alloys were named 'high-boron cast irons' (HBCIs). Regarding the carbon content, they are often called

'steels' [54], although, according to the morphological characteristics of the structure (presence of eutectics), they should be classified as white cast irons. The main advantages of HBCIs are low cost and high abrasive wear resistance, which is competitive with more expensive alloyed Fe–C-based alloys (high-Cr cast irons, high-speed steels, multicomponent cast irons, *etc.*).

3.2. Chemical Composition, Mechanical and Wear/Corrosion Performance of 'High-Boron Cast Irons'

The base high-B cast iron proposed by Lakeland are plain Fe–B–C alloys containing 1.2–3.5 wt.% B and 0.2–0.5 wt.% C [54, 55]. They crystallize according to the ternary Fe–C–B diagram [56], which includes α-Fe, $Fe_3(C, B)$, $Fe_{23}(C, B)_6$, Fe_2B, and graphite (Fig. 5). In the temperature range of 700–800 °C, borocementite is transformed into carboboride $Fe_{23}(C, B)_6$ by the peritectoid reaction $Fe_3(B, C) + Fe \rightarrow Fe_{23}(C, B)_6$ or by its decomposition $Fe_3(B, C) \rightarrow Fe_{23}(C, B)_6 + Fe_2B$ (under an increased B/(C + B) ratio) [56]. In the Fe–C–B alloys, carbon can replace 3–8 at.% B in Fe_2B boride [57], and boron — up to 20 at.% C in the cementite phase [58]. According to Ref. [43], the formation of vacancies during the growth of Fe_2B crystals makes it possible to introduce carbon atoms into the boride lattice, which strengthens the covalent bonding and leads to an increase in (a) the *a* parameter of the crystallite lattice, (b) microstresses, and (c) the density of dislocations. Considering this, it can be assumed that carbon improves the boride's hardness.

High-boron alloys are conventionally obtained by casting in sand moulds. With a low carbon content in cast steels of the Fe–C–B system, a microstructure is formed, which includes hard phases (FeB, Fe_2B and $Fe_2(B, C)$) in the form of boride (carboboride) eutectic network. The alloy matrix in the cast state is ferrite or pearlite, the volume fractions of which are determined by the concentration of carbon in the alloy [59], thus, as-cast HBCIs possess rather low hardness (less than 40 *HRC*). A significant improvement in the properties of the alloy is achieved by high-temperature destabilizing heat treatment (with heating above 900 °C), which causes the secondary carboboride $M_{23}(B, C)_6$ precipitation followed by matrix depletion on carbon with its subsequent transition into martensite. These transformations significantly increase the microhardness of HBCI matrix leading to a bulk hardness increase [59]. The formation of secondary carbides is also possible during the tempering at temperatures above 200 °C [59]. At the same time, a number of studies [60, 61] have shown that the morphology of primary borides does not change during high-temperature heat treatment, which points to their extremely high resistance to dissolution when heated.

In a heat-treated state, HBCIs possess the hardness and impact toughness of 55–63.5 *HRC* and 6.5–15.5 $J \cdot cm^{-2}$, respectively, as shown

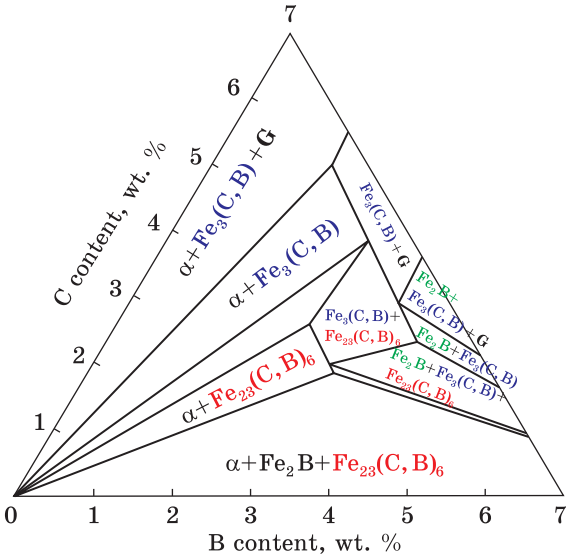

Fig. 5. Isothermal (700 °C) cross-section of the ternary Fe–C–B system [56]

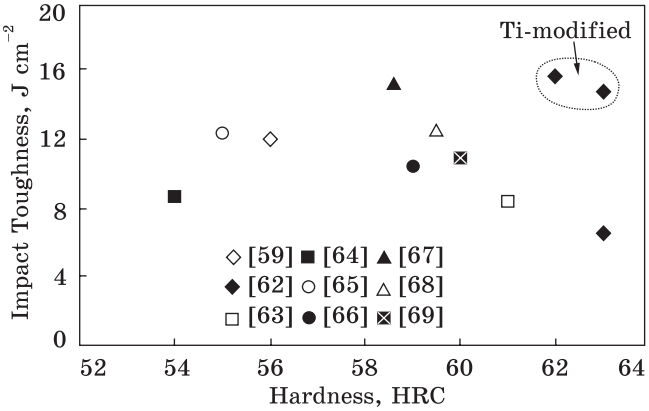

Fig. 6. 'Hardness-impact toughness' correlation for high-B cast irons: high-B HSS [62], Fe–B–C alloys [59]–[66], Fe–B–C–Cr alloys [67]–[69]

in Fig. 6 [59–69]. As seen, there is no specific correlation between these parameters. The boride morphology and distribution are more relevant: modification by titanium led to a 2-fold increase in impact toughness at the same hardness due to boride refinement [68]. The data presented in Fig. 6 coincide with Lakeland's conclusions that hardness and impact toughness of high-boron cast irons may vary within 22–62 *HRC* and 8–15 J·cm^{-2}, respectively [55].

The 'two-body abrasion' wear performance of Fe–C–B high-boron alloys was analysed in Ref. [70] in comparison with conventional cast alloys. It was established that the abrasive resistance of alloys is controlled by the carbon and boron contents. At their low concentrations (0.2–0.4 wt.% C, 1.0 wt.% B), the wear resistance of the alloy is lower as compared to high chromium cast iron. With an average carbon content

(0.3–0.45 wt.%) and a high boron content (1.5–3.0 wt.% B), the wear resistance of high-boron alloy significantly exceeds the wear resistance of high-chromium cast iron. The wear resistance of Fe–C–B alloys with high contents of carbon (0.5–1.0 wt.%) and boron (2.0 wt.%) is also higher than that of high-Cr cast iron [70, 71].

As reported in Ref. [66], under the 'two-body abrasion' test the Fe–B–C alloys (0.08–0.2 wt.% C, 2.2–4.0 wt.% B) had an advantage over Ni-hard cast iron and hardened steels GCr15 (ШХ15) and Cr12MoV (Х12МФ) being close to the level of high chromium cast iron Cr15Mo3. Similar data were obtained in Ref. [72], where authors established that Fe–C–B alloys (0.1–0.25 wt.% C, 0.8–1.2 wt.% B), hardened to 56 *HRC*, were as wear-resistant as high-chromium cast iron (15 wt.% Cr, 62.5 *HRC*) performing a doubled advantageous before martensitic steel (0.32 wt.% C, 2.11 wt.% Cr, 0.97 wt.% Mo) with a hardness of 51 *HRC*. Considering the high tribological properties of high-boron steels, they are successfully used for the manufacture of wear-resistant and corrosion-resistant parts, for example, liners of ball mills [73], rolling mill guides [74], hammerheads for crushers [75], grinding balls [61], *etc.*

Apart from high wear resistance, HBCIs demonstrate an advanced corrosion/erosion resistance in the molten Zn and Al [76–78]. This property is relevant for the parts of hot-deep galvanizing equipment, which suffer corrosion attacks from molten metals. The advanced corrosion behaviour of HBCIs is governed by two structural factors: (a) the presence of Fe_2B borides, which are not wetted by molten zinc [76], and (b) the presence of a discontinuous boride network that prevents the direct reaction of Fe with liquid Zn (Al). Due to these factors, the corrosion resistance of Fe–B alloys with different boron concentrations (1.5–6.0 wt.%) is about 5 times higher compared to the corrosion resistance of 18–8 stainless steel [79, 80]. With that, the corrosion resistance increased considerably when the boron content increased from 1.5 to 3.5 wt.%; under further boron content increase, the corrosion rate decreased insignificantly.

The corrosion resistance of Fe–B alloys in molten zinc is controlled by boride orientation relatively Fe/Zn interface. The authors of [80] investigated the corrosion resistance of directly solidified HBCIs and reported that Fe–B alloy with borides Fe_2B oriented perpendicular to the corrosion surface showed higher corrosion resistance than alloys with borides of parallel orientation or in the form of a eutectic network. This behaviour was explained by the formation of an interface-pinning multilayer, which appeared as a reaction of the columnar borides with the corrosion products (the epitaxial compound ζ-$FeZn_{13}$) (Fig. 7, *b*). In the pinning multilayer, the borides and ζ-$FeZn_{13}$ are connected through the orientation relationships $(001)Fe_2B \| (-402)\zeta$-$FeZn_{13}$ and $(002)Fe_2B \| (110)$ ζ-$FeZn_{13}$ that allows them to slow down the diffusion and infiltration of

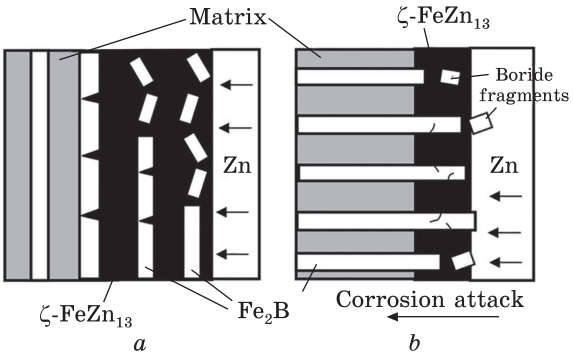

Fig. 7. The erosion–corrosion mechanism of directionally solidified Fe–3.5 wt.% B alloys in molten zinc: *a* — Fe_2B borides are parallel to the interface, *b* — Fe_2B borides are perpendicular to the interface (pinning effect). (Constructed based on the date in Ref. [81].)

liquid zinc to Fe-matrix. In addition, the strong pinning effect is induced by the geometric constraints from oriented borides and volume expansion from corrosion products. With increasing the spacing between Fe_2B lamellas higher than 3–3.5 μm, the pinning effect diminishes. Within the pinning layer, borides suffer the stresses followed by the cracks formation and breakage.

The mechanism of corrosion of nonoriented boride network is its proliferation by the corrosion products (Fe–Zn) with further fracture. The parallel-oriented borides are also proliferated by zinc flow with the formation of many small granular corrosion products at the interface Fe/liquid Zn. Accumulation of these products triggers the 'layer-by-layer' detachment of the columnar borides from the matrix (Fig. 7, *a*) [81]. Due to the difference in corrosion mechanisms, the corrosion rate of Fe–3.5 B alloy is ranged as follows: perpendicular oriented Fe_2B → vertical oriented Fe_2B (+41.7 %) → non-oriented Fe_2B (+9.6 %).

Chromium is known as the most important element for corrosion inhibition. The feasibility of Cr addition to Fe–C–B alloys to improve their corrosion resistance was evaluated by Ma *et al.* [82] who studied the corrosion behaviour of Fe–3.5 B alloy in molten zinc under different Cr contents (up to 18 wt.%). The remarkable improvement of corrosion resistance was found when Cr content was 2–5 wt.% with maintaining borides' network morphology. At higher Cr content, the corrosion resistance even slightly decreased due to the breaking of the boride network continuity [83]. This finding shows the importance of 3*D* boride skeleton for HBCIs' resistance in molten Zn (Al). Thus, a high Cr content is ineffective for Fe–C–B alloys for these corrosion applications.

3.3. Control of the Borides' Size and Morphology

The main disadvantage of high-boron alloys is their high brittleness due to a continuous eutectic skeleton [84]. Furthermore, due to the weak B–B bond along the [002] direction, boride Fe_2B is a rather brittle phase [85], which leads to the tendency of borides to crack and pill-off during

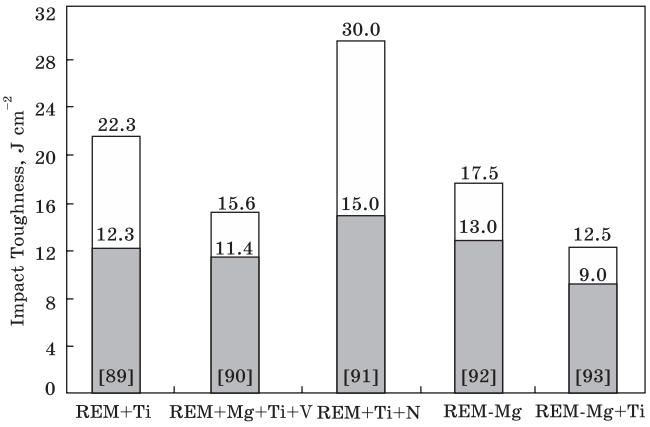

Fig. 8. Effect of modification on impact toughness of Fe–B–C alloys (grey — unmodified, light — modified) [89–93] (each column contains reference, where the information was adopted from)

wear. The HBCIs' toughness can be increased by 'breaking' the eutectic network and changing Fe_2B size and morphology. For this purpose, the following approaches have been assayed: (a) modifying the melt with rare-earth metal (REM) additives, (b) adding the alloying element to control the crystallization process, (c) heat treatment, (d) hot plastic deformation [86–88]. Heat treatment is not appropriate to destroy the boride network, since borides do not dissolve in the matrix due to the very low boron solubility in iron. REM-modification was proved more effective for Fe–C–B alloys. Figure 8 presents the impact toughness improvement by using different modification additives (REM + Ti, REM–Mg + V + Ti, REM + Ti + N, REM–Mg, REM + Ti + Mg, REM–Mg + Ti, *etc.*) confirming the increase in impact toughness in all modified alloys, while their hardness was close to that of unmodified alloys [89–93]. Modification led to the refinement of borides, besides places with thinning ('necking') of the eutectic network appeared beneficial for easier network destruction [70].

The most effective method of boride network breaking is a hot plastic deformation [94, 95]. Zhang *et al.* [94] found that the impact toughness of HBCI containing 0.35 wt.% C and 0.38 wt.% B can be increased approximately 20 times (from 5 J·cm^{-2} to 107 J · cm^{-2} at 54 *HRC*) by forging. Hot deformation with a forging ratio of 4–8 resulted in a complete fracture of the eutectic network with a more uniform distribution of borides (in the form of network fragments) in the alloy volume (Fig. 9) [94]. Zhang *et al.* [94] explained the ability of high-boron alloys to be forged without breakage (unlike white cast irons) by the sliding and accumulation of dislocations inside the borides, which causes their easy fracture during deformation without the macrocracks formation [94]. Moreover, it was established that hot plastic deformation stimulates the spheroidization of boride fragments due to the internal diffusion of boron along the boundaries of subgrains formed under deformation [94]. He *et*

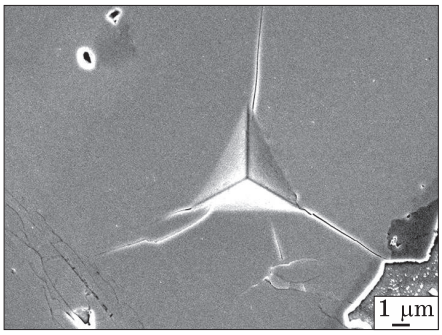

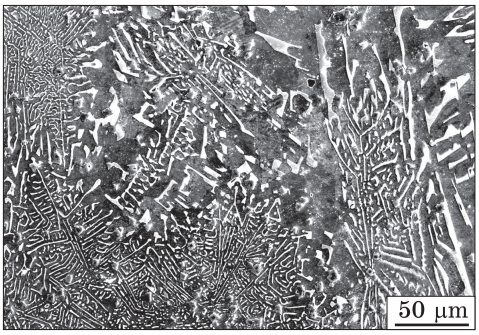

Fig. 9. Imprint-oriented cracks on boride M_2B after the nanoindentation with a load of 500 mN

Fig. 10. The 'Chinese script' eutectic ($\alpha + M_2(B, C)_5$) in a 'hybrid' multicomponent high-B alloy

al. [95] used hot rolling to process Fe–1.8 wt.% B alloy with Ti addition (up to 6.0 wt.%) and obtained very promising results: the elongation of the alloys increased from 0.6–4.0% in the as-cast state to 7.0–16.2% after hot rolling (the higher values are attributed to Ti-alloyed alloys). It is noteworthy that impact toughness (U-notched specimens) of the rolled alloy with 4 wt.% Ti reached 213 $J \cdot cm^{-2}$. The best combination of the mechanical properties was obtained at an atomic percent relation of Ti/B = 0.5, which referred to the substitution of Fe_2B network by dispersed precipitations of titanium boride TiB_2.

With boron content increase, the efficiency of hot deformation decreases. In alloys containing 0.35–0.45 wt.% C and 1.0–1.5 wt.% B (also 1.5–2.0 wt.% Cr, 0.4–0.5 wt.% Mo), the multiaxial forging technique allowed to increase the impact toughness from 4 $J \cdot cm^{-2}$ to 29.4 $J \cdot cm^{-2}$ [96]. Furthermore, in Fe–C–B alloy containing 0.36 wt.% C and 1.48 wt.% B, forging led to increase in impact toughness from 4.5 $J \cdot cm^{-2}$ (as-cast state) to 9.3 $J \cdot cm^{-2}$ (after quenching from 1050 °C to 58 *HRC*) [95]. The authors [95] explain the positive effect of hot deformation by the destruction of the boride network, changing the boride morphology and reducing their size, and strengthening the matrix.

Hot deformation controversially affects the wear resistance of HBCIs. In the 'two-body abrasion' test conditions, the wear resistance of deformed Fe–B–C alloys (having broken boride networks) was found to be lower than that of the same alloys with eutectic boride skeleton. This refers to the load transfer from the abrasive particles to the underlying matrix: unbroken boride skeleton ensures better load distribution preventing the stress concentration [96]. In contrast, under the 'three-body abrasion' test, Fe–B–C alloys with broken boride network perform better

wear resistance than that of Fe–B–C alloys with network borides [71]. Yi *et al.* [97] compared a 'three-body abrasion' wear resistance of Fe–B alloy obtained by deferent casting technologies (semi-solid and ordinary cast). They revealed that semi-solid alloy had a finer boride phase, which transformed into the short rod-shaped and round borides under heat treatment. This change in boride morphology caused a lower wear rate of semi-solid Fe–B cast alloy as compared to ordinary cast alloy.

3.4. Effect of Alloying on the High-Boron Alloys' Properties

It is known that alloying is an effective way of controlling the structure and properties of steel and cast iron. This aspect was extensively explored in many works [98–115] devoted to the effect of Cr, W, Mo, Ti, and other elements on the properties of high-boron cast irons. Chromium is more often in the focus concerning Fe–B–C alloys [98–101]. Lentz *et al.* [99] studied the effect of chromium in the range of 0–55 at.% on the structure of Fe–5 wt.% B alloy. They showed that as the Cr content increases, the M_2B boride changes its crystal structure: (a) in the range of up to 14.7 at.% Cr, boride $(Fe, Cr)_2B$ has a tetragonal lattice, (b) in the range of 14.7–23.2 at.% Cr, there is a transition $(Fe, Cr)_2B$ (tetragonal) → $(Cr, Fe)_2B$ (orthorhombic); (c) at a higher Cr concentration, boride has an orthorhombic lattice. This was ascribed to Cr solution in F_2B boride: the chromium concentration in F_2B gradually increased with an increase in total Cr content in the alloy (it reached 71 wt.% at 50 wt.% Cr within the alloy bulk). For characterization of boride micromechanical properties, the authors of [99] used the nanoindentation testing with further fracture toughness calculation according to Eq. (9):

$$K_{IC} = x_v \sqrt{\frac{a}{l}} \left[\frac{E}{H}\right]^{2/3} \frac{P}{c^{3/2}}, \qquad (9)$$

where E is elastic modulus, H is hardness, P is a load, c and l are the crack length measured from the centre and the corner of the indentation imprint, respectively (Fig. 9), a is half of the imprint diagonal, x_v is a calibration constant.

It was found that adding 5 at.% Cr slightly increased the fracture toughness of M_2B boride from 3.15 MPa·m$^{1/2}$ to 3.5 MPa·m$^{1/2}$. A further increase in the Cr content to 14.7 at.% led to a decrease in toughness to 2.1 MPa·m$^{1/2}$ due to the polytrophic 'tetragonal → orthorhombic' transition (which introduces lattice distortion in the major tetragonal M_2B phase [102]). The presented data are partially confirmed by the results of work [95] showing that the fracture toughness of boride Fe_2B in the Fe–3 wt.% B–Cr system is maximum at a chromium content of 2.0 wt.%. This was explained by the change in the interplanar distances of two perpendicular crystal planes ((002) and (200)), when Cr is added.

A decrease in the fracture toughness of boride M_2B with a Cr content of 5–15 at.% was also observed in Refs. [100, 101].

Within the tetragonal M_2B phase, chromium slightly increases hardness and elastic modulus that can be referred to strengthening a B–B bond in [002] direction under Cr doping [103] owing to orbital hybridization between Cr and B [101]. This Cr behaviour can be also resulted from the decrease in surface energy and the increase in interplanar spacing in (200) planes under the Cr effect [100].

Within the orthorhombic M_2B phase, the increase in Cr content is followed by a strong progressive increase in hardness, elastic modulus, and fracture toughness. As shown by *ab initio* calculations [104], a hybridization of Cr*d* and B*p* states results in strong covalent Cr–B and Cr–Cr bonds within the layered orthorhombic M_2B lattice (three Cr layers and one B layer), while a B–B bond within boron layer is weak. Interestingly, the strongest bond is associated with axis *c* in [001] direction [105], while the parameter *c* decreases with Cr content increase [106]. At 55 at.% Cr, hardness and elastic modulus of orthorhombic boride M_2B reached 27 GPa and 473 GPa, respectively, exceeding the values for tetragonal boride [99]; fracture toughness reached 3.2 MPa·m$^{1/2}$ [99]. A similar effect of Cr on M_2B boride properties was reported by Lentz *et al.* [107] for Fe–(up to 25 wt.% Cr)–Mn–C–B cast irons and by Ma *et al.* [98] for Fe–3.5 wt.% B–(up to 18 wt.% Cr) alloys.

The effect of Ti, V, Mn, Co, Ni, and Cu on mechanical, electronic, and magnetic properties of Fe_2B boride were investigated in [108] based on the 'First-Principles Calculations' approach. It was concluded that all the mentioned elements, except for manganese, increase the fracture toughness of Fe_2B boride. In contrast, Jian *et al.* [109] experimentally showed that the introduction of 2.0 wt.% Mn to Fe–3 wt.% B alloy positively influences the fracture toughness of this boride. Ni and Cu increase the hardenability of high-boron steels improving their hardness and impact toughness [110, 111]; however, an excess of Cu (more than 2 wt.%) reduces the hardness and wear resistance of the alloy due to the formation of pearlite. The latter is attributed to the segregations of Cu atoms resulting in body-centred Cu nanoprecipitations acting as heterogeneous nuclei for the pearlite colonies [111].

According to [112], the addition of titanium into the Fe–1.8 wt.% B alloy leads to refining M_2B borides and breakage of the eutectic network. An increase in Ti content to the atomic ratio Ti/B = 0.5 leads to full substitution of M_2B boride network by disperse TiB_2 inclusions achieving a significant enhancement of ductility and impact toughness [95, 112]. With that, it should be bearing in mind that the net-like $M_2B \rightarrow$ dispersed TiB_2 transition is accompanied by decreasing in boride volume fraction (1.8 wt.% B corresponds to 20.4 wt.% Fe_2B and only to 5.8 wt.% TiB_2 [100]) that can deteriorate the wear resistance.

Adding chromium into the Fe–C–B alloys may result in a structure very different from continuous eutectic network. Under higher Cr content (≥20 wt.%), the Cr-based $M_7(C, B)_3$ and $M_{23}(C, B)_6$ carboborides crystallize as eutectic having the specific for high-Cr cast iron inverted morphology which is more appropriate for impact toughness. Hartono *et al.* [113] explored (in wt.%) Fe–(25–30) Cr–(0.3–3.5) C–(0–2.4) B with the eutectic composition. The structure of the alloys consisted of the following eutectics: (a) $(\delta + M_2B)$ at 0 wt.% C–2.2 wt.% B, (b) $(\gamma + M_2B)$ and $(\gamma + M_{23}(C, B)_6)$ at 0.6 wt.% C–2.0 wt.% B and 1.5 wt.% C–1.5 wt.% B, (c) $(\gamma + M_7(C, B)_3)$ and $(\gamma + M_{23}(C, B)_6)$ at 2.2 wt.% C–1.0 wt.% B, (d) $(\gamma + M_7(C, B)_3)$ at 2.8 wt.% C–0.5 wt.% B and 3.5 wt.% C–0 wt.% B. All the as-cast alloys performed the compressive strength of above 2000 MPa at room temperature and above 100 MPa at 800 °C. After quenching followed by secondary carboboride precipitation, the matrix hardness of most alloys is increased to 950–1020 *HV*.

The influence of W, Mo, and Al on the properties of Fe_2B boride is described in works [114–116]. Addition of 2.0 wt.% W increases the fracture toughness of Fe_2B boride in as-cast Fe–B–C alloy by more than 80% [115]. The replacement of iron with molybdenum in the Fe_2B crystalline lattice leads to an increase in bonding strength and thermodynamic stability [116]. At a certain M/B ratio in the alloy (where M is Mo and W), boride M_2B_5 may appear instead of M_2B [117]. Adding up to 1.8 wt.% Al in high-speed steel with 1.50 wt.% B and 0.40 wt.% C does not change the properties of boride M_2B, but it causes refinement of the eutectic network leading to a 1.5-fold increase in impact toughness [114]. The addition of chromium also increases the impact toughness of high-boron steels by the formation of a ductile bainite matrix [80].

4. Hybrid Approaches in the Design of Tribological Alloys

Encouraging data on the effect of boron on tribological properties of Fe–C alloys resulted in a number of hybrid approaches to develop B-containing wear-resistant alloys of a new generation such as B-added tool stamping steels [107], B-added austenitic stainless steels [118], B-added high-Cr cast irons [113], high-B HSSs [119].

Considering the positive effect of strong carbide-forming elements on HBCIs' properties, the high-boron high-speed steels were developed by combining the concepts of 'multicomponent cast irons' and 'high-boron cast irons'. They are Fe–C–B alloys with additions of Mo (W)–V–Cr–Al complex [111, 119]. Thus, Ren *et al.* [62] studied HSS of chemical composition (in wt. %) Fe–2 B–0.4 C–6 Cr–4 Mo–2 Al–1 Si–1 V–0.5 Mn. High-B HSSs contain carboboride phases ($M_2(B, C)$, $M_3(B, C)$, $M_{23}(B, C)_6$), which are harder than those in Fe–C–B and Fe–C–B–Cr alloys [114, 119]. Adding Al increases the high-temperature wear/corrosion resis-

tance of high-B steel due to the formation of a protective Al_2O_3 oxide film [119]. Ma *et al.* [120] investigated 2.0 wt.% B–0.4 wt.% C HSS doped with 4.8 wt.% Cr, 1.2 wt.% W, 0.5 wt.% V, 0.65 wt.% Mo, where Al content varied up to 1.79 wt.%. The result of this study showed that Al promoted the formation of pearlite and ferrite in an as-cast state. With that, Al promoted an increase in hardness under the destabilizing heat treatment (up to 64 *HRC* at 1.2 wt.% Al). Furthermore, Al stimulated the precipitation hardening due to $M_{23}(B, C)_6$ and $M_6(B, C)$ precipitates formation at tempering (520 °C). The highest secondary-hardening effect was observed at 0.6 wt.% Al.

An interesting research was presented in article [121] dedicated to the evaluation of high-temperature abrasive resistance of high-B HSS containing 0.4–0.5 wt.% C, 1.5–1.8 wt.% B, 4–5 wt.% Cr, 1.2–1.8 wt.% Mo, 0.6–1.0 wt.% W, 0.6–1.0 wt.% V. The study showed that the high-temperature (500 °C) wear resistance of this HSS was 2.3 times higher than that of conventional HSS (1.8 wt.% C, 4.5 wt.% Cr, 5 wt.% Mo, 2 wt.% W, 4 wt.% V) and 1.5 times than 25 wt.% Cr-cast iron. These results proved the great potential of high-B HSS, especially taking into account its lower cost as compared to conventional HSSs. This conclusion is supported by the study [122], where high-boron HSS (0.54 wt.% C, 1.96 wt.% B, 5.23 wt.% Cr, 7.06 wt.% Mo, 3.82 wt.% W, 2.62 wt.% Al) was stated as a cheap replacement for very expensive hard alloys: when used in hot rolling wire mills, its wear rate was 0.26 mm/one thousand tons to be close to that of powder-metallurgy cemented carbide alloy. Notably, the cost of high-boron HSS was just 28% to that of hard alloy.

According to Lentz *et al.* [107], the Fe–0.4 C–1 B–(2.5–10) Cr (in wt.%) steel produced by casting and hot rolling performed a higher combination of impact toughness, bending strength, wear resistance, and hardness as compared to conventional tool steel X153CrMoV12-1 for cold deformation. With that, the cost of high-boron steel is 52–72% lower than that of X153CrMoV12-1.

Despite of obvious advantages of high-boron cast irons, their lower impact toughness remains to be a serious problem caused by net-like boride distribution, which affects the tools' service life. The eutectic network can be completely broken by hot forging/rolling [96], but this technology is applicable only for a relatively low volume fraction of the boride phase, otherwise, it leads to forging cracking. As shown in Ref. [123], the powder metallurgy using the fast-crystallized powder allows overcoming this problem achieving promising mechanical properties at a higher boride volume fraction.

Another way to resolve this problem is by adding the strong carbide-forming elements (Ti, Nb, Zr, V), which form *M*C carbide with a cubic lattice [124]. These elements are frequently used to control the micro-

structure and tribological behaviour of alloyed cast irons [125]. As shown in Ref. [126], the addition of 2 wt.% Nb and 2 wt.% Ti significantly improves the wear resistance of high-Cr cast iron. Similar results were obtained by Kusumoto *et al.* [127] who revealed a doubled increase in 'two-body abrasion' wear resistance of multicomponent cast iron (in wt.%) Fe–2 C–5 Cr–5 Mo–5 W due to the addition of 3 wt.% Nb. The same amount of Nb added to (in wt.%) Fe–0.5 C–2.0 B–4.2 Cr alloy increased the bending strength from 1304 MPa to 1731 MPa and the fracture toughness from 29.8 $m^{1/2}$ to 32.9 $MPa \cdot m^{1/2}$ [128]. Having a high affinity for carbon (boron) titanium bind, a significant amount of C and B with the formation of compounds MC (M_xB_y), which crystallize at high temperatures in the form of compact cubical precipitates. When titanium is introduced into high-Cr cast iron, TiC carbide crystallizes at a higher temperature due to low Gibbs energy and low solubility in the melt [62]. TiC carbide acts as a substrate for eutectic M_7C_3 carbide due to the proximity of lattice parameters [124, 129–131]. The heterogeneous nucleation results in discontinuity of the eutectic network and the refinement of M_7C_3 carbide. The same behaviour is expected, if Ti is introduced to high-boron alloys. The ability of a compound to act as a nucleus can be assessed by the misfit degree (δ), which should be lower than 12%. The value of δ is calculated as follows [62] (see also Ref. [88] and references therein):

$$\delta_{(hkl)n}^{(hkl)s} = \sum_{i=1}^{3} \frac{1}{3} \frac{\left| d[uvw]_S^i \cos\vartheta - d[uvw]_n^i \right|}{d[uvw]_n^i} \cdot 100\%, \qquad (10)$$

where s and n refer to nucleus and crystalline phases, (hkl) is a crystallographic plane, $[uvw]$ is a crystal orientation, d is interatomic distance along $[uvw]$, θ is an angle between $[uvw]_S$ and $[uvw]_n$.

The calculations performed by Ren *et al.* [62] showed that the misfit degree for the relationship (110)TiC ∥ (110)M_2(B, C) is 9.3%. This means that carbides TiC can effectively act as heterogeneous nuclei for the carboboride M_2(B, C), thus, preventing the formation of a continuous boride network and improving the mechanical properties of Fe–B alloys. Another important issue is that Ti-based compounds (borides, carbides) are characterized by much higher hardness as compared to those formed by W, Mo, V, and Cr (see Table). This makes the Ti-alloying of high-boron alloys a promising direction for designing new wear-resistant materials containing very hard precipitates in their structure. Such alloys can be a feasible option for industrial applications where the raw materials of high hardness and abrasiveness (Al_2O_3, SiC, B_4C, *etc.*) are processed.

The steps in this direction have been already taken in Ref. [132], where the authors proposed a 'hybrid; approach is based on the concepts of 'multicomponent cast irons' and 'high-boron cast iron' combined with

a titanium addition. It was deduced that the hybrid multicomponent high-B alloys ((in wt.%) Fe–B–C–5 W–5 Mo–5 V–10 Cr–2.5 Ti) acquire the structure presenting no continuous eutectic network. In the alloy containing 0.7 wt.% C and 1.5 wt.% B, a fan-like eutectic ($\alpha + M_2(B, C)_5$) of 'Chinese script' morphology was observed to be the major in the structure. This morphology features the non-connected carboboride fibres radiating within the metallic matrix from the centre of a eutectic colony (Fig. 10). Such boride distribution is beneficial for impact toughness due to the absence of a brittle network skeleton. Apart from a carboboride $M_2(B, C)_5$, other hard compounds (TiC, Ti(C, B), $M_7(C, B)_3$, $M_3(C, B)$) were also present in minor amounts. The concept of the 'hybrid' high-B multicomponent alloys needs to be further developed in terms of optimizing their chemical composition and assessing the mechanical and tribological properties taking into account the 'cost-property' ratio.

5. Conclusions

The abrasion of the working surfaces of machines parts and tools remains a permanent problem bringing colossal economic losses in many spheres of production. The widely applied conventional wear-resistant materials have a limited working life caused by the inappropriate hardness of strengthening phases present in their structure (1000–1800 *HV*). An effective way to diminish abrasive wear of the cast components is the use of novel wear-resistant materials with optimized tribomechanical behaviour.

The main vision is the creation of a heterophase structure comprising the hard phases of different types (carbides, borides, and carboborides) distributed within a martensite matrix strengthened by secondary precipitates. The multialloying with several strong carbide-forming elements enables their competition to bind with carbon that leads to refinement of the structural elements with a sequential increase in mechanical/wear behaviour. Multicomponent cast irons follow this approach being alloyed with W, Mo, V, and Cr in equal proportions to provide the structure comprising different sets of eutectic carbides (MC, M_2C, M_6C, M_7C_3) depending on carbon and chromium contents. After heat treatment, the multicomponent cast irons performed 4–5 times higher abrasive wear resistance compared to conventional cast materials (Ni-hard, high-Cr cast iron, *etc.*)

Currently, the attention of the researchers is attracted by the perspectives of significant wear resistance enhancement through the alloying by a higher amount of boron (up to 1–3.5 wt.%). The novel class of cast irons (Fe–B–C-'high-boron cast irons') was recently developed to surpass the traditional F–C-based cast alloys in abrasive performance with simultaneous reducing production costs. This became possible due to the

formation of boride and carboboride phases (Fe_2B, $Fe_3(C, B)$, M_2B, $M_2(B, C)$), which are harder than corresponding carbide phases. High-B cast irons show advanced corrosive resistance in liquid metals (Zn, Al) due to the 3*D*-dimension skeleton of boride eutectic. However, the continuous boride network significantly reduces impact toughness; therefore, different techniques are applied (REM–Mg modification, fast solidification and powder metallurgy, hot deformation, *etc.*) to break the network in order to improve the mechanical properties.

The most perspective is a 'hybrid' approach consisting of a combination of different concepts to design the new-generation wear-resistant materials with advanced tribological behaviour. In accordance with this trend, the novel alloys were currently designed based on the addition of alloying elements (W, Mo, V, Cr, Al, and Ti) into Fe–C–B alloys specifically: high-boron high-speed steels, high-boron cold work tool steels, high-boron stainless steels, *etc.* High-boron ('hybrid') multicomponent cast irons are the recent developments in the field of functional cast wear-resistant materials for tribological applications.

Acknowledgement. The work contains results of the study carried out within the framework of the project 'Development of hybrid multicomponent alloys for tribotechnical purposes and technologies for their structural modification using highly concentrated energy sources' (State Reg. No. 0122U000325) funded by the Ministry of Education and Science of Ukraine.

REFERENCES

1. K. Holmberg and A. Erdemir, *Friction*, **5**, No. 3: 263 (2017); https://doi.org/10.1007/s40544-017-0183-5
2. E. Badisch and C. Mitterer, *Tribol. Int.*, **36**, No. 10: 765 (2003); https://doi.org/10.1016/S0301-679X(03)00058-6
3. J. Rendyn and M. Olsson, *Wear*, **267**, No. 11: 2055 (2009); https://doi.org/10.1016/j.wear.2009.08.005
4. N. Ojala, K. Valtonen, V. Heino, M. Kallio, J. Aaltonen, P. Siitonen, and V.T. Kuokkala, *Wear*, **317**, Nos. 1–2: 225 (2014); https://doi.org/10.1016/j.wear.2014.06.003
5. A.D. Koval', V.G. Efremenko, M.N. Brykov, M.I. Andrushchenko, R.A. Kulikovskii, and A.V. Efremenko, *J. Frict. Wear*, **33**. No. 1: 39 (2012); https://doi.org/10.3103/S1068366612010072
6. M. Shah and S.D. Bakshi, *Wear*, **402**, No. 11: 207 (2018); https://doi.org/10.1016/j.wear.2018.02.020
7. M.O. Vasylyev, S.I. Sidorenko, S.M. Voloshko, and T. Ishikawa, *Usp. Fiz. Met.*, **17**, No. 3: 209 (2016); https://doi.org/10.15407/ufm.17.03.209
8. Y. Chabak, V. Efremenko, V. Zurnadzhy, V. Puchy, I. Petryshynets, B. Efremenko, V. Fedun, K. Shimizu, I. Bogomol, V. Kulyk, and D. Jakubeczyova, *Metals*, **12**, No. 2: 218 (2022); https://doi.org/10.3390/met12020218

9. Y.X. Ye, C.Z. Liu, H. Wang, and T.G. Nieh, *Acta Mater.*, **147**: 78 (2018); https://doi.org/10.1016/j.actamat.2018.01.014
10. D. Zhang, C. Kenel, and D.C. Dunand, *Acta Mater.*, **221**: 117420 (2021); https://doi.org/10.1016/j.actamat.2021.117420
11. Y.G. Chabak, V.I. Fedun, K. Shimizu, V.G. Efremenko, V.I. Zurnadzhy, and K. Shimizu, *Probl. At. Sci. Technol.*, **104**, No. 4: 100 (2016).
12. M.O. Vasylyev, B.M. Mordyuk, S.M. Voloshko, V.I. Zakiyev, A.P. Burmak, and D.V. Pefti, *Metallofiz. Noveishie Tekhnol.*, **41**, No. 11: 1499 (2019) (in Ukrainian); https://doi.org/10.15407/mfint.41.11.1499
13. Z.A. Duriagina, M.R. Romanyshyn, V.V. Kulyk, T.M. Kovbasiuk, A.M. Trostianchyn, and I.A. Lemishka, *J. Achiev. Mater. Manuf. Eng.*, **100**, No. 2: 49 (2020); https://doi.org/10.5604/01.3001.0014.3344
14. H.Q. Wu, M. Hashimoto, N. Sasaguri, and Y. Matsubara, *Jpn. Foundry Eng. Soc.*, **68**, No. 8: 637 (1996) (in Japanese); https://doi.org/10.11279/jfes.68.637
15. H. Wu, N. Sasaguri, M. Hashimoto, and Y. Matsubara, *Jpn. Foundry Eng. Soc.*, **69**, No. 11: 917 (1997); https://doi.org/10.11279/jfes.69.917
16. M. Hashimoto, O. Kubo, and Y. Matsubara, ISIJ Int., 44, No. 2: 372 (2004); https://doi.org/10.2355/isijinternational.44.372
17. Y. Yokomizo, N. Sasaguri, K. Nanjo, and Y. Matsubara, *Jpn. Foundry Eng. Soc.*, **74**, No. 1: 9 (2002) (in Japanese); https://doi.org/10.11279/jfes.74.9
18. Y. Matsubara, *Research and Development of Abrasion Wear Resistant Cast Alloys for Rolls of Rolling and Pulverizing Mills* (Kurume: 2002), p. 30.
19. W.M. Pasini, M.R. Belle, L. Pereira, R.F. do Amaral, and V.K. de Barcellos, *Mater. Res.*, **24**, No. 2: e20200398 (2021); https://doi.org/10.1590/1980-5373-MR-2020-0398
20. Y. Matsubara, N. Sasaguri, and K. Shimizu, *Wear*, **250**, Nos. 1–12: 502 (2001); https://doi.org/10.1016/S0043-1648(01)00599-3
21. J. Opapaiboon, M.S.N. Ayudhaya, P. Sricharoenchai, S. Inthidech, and Y. Matsubara, *Mater. Trans.*, **60**, No. 2: 346 (2019); https://doi.org/10.2320/matertrans.M2018318
22. J. Opapaiboon, P. Sricharoenchai, S. Inthidech, and Y. Matsubara, *Mater. Trans.*, **56**, No. 5: 720 (2015); https://doi.org/10.2320/matertrans.M2015001
23. S. Inthidech and Y. Matsubara, *Int. J. Metalcast.*, **14**, No. 1: 132 (2020); https://doi.org/10.1007/s40962-019-00343-y
24. Y.P. Wang, D.Y. Li, L. Parent, and H. Tian, *Wear*, **271**, Nos. 9–10: 1623 (2011); https://doi.org/10.1016/j.wear.2010.12.029
25. Y. Zhang, K. Shimizu, X. Yaer, K. Kusumoto, and V.G. Efremenko, *Wear*, **390–391**: 135 (2017); https://doi.org/10.1016/j.wear.2017.07.017
26. V.G. Efremenko, K. Shimizu, A.P. Cheiliakh, T.V. Pastukhova, Yu.G. Chabak, and K. Kusumoto, *Int. J. Miner., Metall. Mater.*, **23**, No. 6: 645 (2016); https://doi.org/10.1007/s12613-016-1277-1
27. K. Kusumoto, K. Shimizu, V.G. Efremenko, H. Hara, M. Shirai, J. Ito, M. Hatate, Y. Gaqi, and R.H. Purba, *Wear*, **426–427**: 122 (2019); https://doi.org/10.1016/j.wear.2019.01.108
28. Y. Zhang, K. Shimizu, K. Kusumoto, K. Tamura, H. Hara, and J. Ito, *Mater. Trans.*, **58**, No. 6: 927 (2017);

https://doi.org/10.2320/matertrans.F-M2017810
29. T. Meebupha, S. Inthidec, P. Sricharoenchai, and Y. Matsubara, *Mater. Trans*, **58**, No. 4: 655 (2017);
https://doi.org/10.2320/matertrans.M2016396
30. *Konstrukcionnye Materialy: Spravochnik* [Structural Materials: Handbook] (Ed. B.N. Arzamasov) (Moskva: Mashinostroenie: 1990) (in Russian).
31. T. Sasaki, T. Yakou, M. Umemoto, and Y. Todaka, *Wear*, **260**, Nos. 9–10: 1090 (2006);
https://doi.org/10.1016/j.wear.2005.07.010
32. G. Shafirstien, M. Bamberger, M. Langohr, and F. Maisenhalder, *Surf. Coat. Technol.*, **45**, Nos. 1–3: 417 (1991);
https://doi.org/10.1016/0257-8972(91)90251-Q
33. I.R. Shein, N.I. Medvedeva, and A.L. Ivanovskii, *Physica B*, **371**, No. 1: 126 (2006);
https://doi.org/10.1016/j.physb.2005.10.093
34. U. Sen, S. Sen, and F. Yilmaz, *J. Mater. Process. Technol.*, **148**, No. 1: 1 (2004);
https://doi.org/10.1016/j.jmatprotec.2004.01.015
35. L.J. Xu, G.S. Zhang, J.W. Li, Z.W. Dong, and S.Z. Wei, *Adv. Mater. Res.*, **189–193**: 3968 (2011);
https://doi.org/10.4028/www.scientific.net/AMR.189-193.3968
36. H. Yang, X.X. Wang, and J.B. Qu, *J. Iron Steel Res. Int.*, **21**, No. 8: 787 (2014);
https://doi.org/10.1016/S1006-706X(14)60142-4
37. Y.X. Li, Z.L. Liu, and X. Chen, *Int. J. Cast Met. Res.*, **21**, Nos. 1–4: 67 (2008);
https://doi.org/10.1179/136404608X361684
38. V.G. Efremenko, K.M. Wu, K. Shimizu, I. Petryshynets, B.V. Efremenko, H. Halfa, Yu.G. Chabak, A.A. Malyshevskyi, and V.I. Zurnadzy, *Practical Metallography*, **57**, No. 10: 714 (2020);
https://doi.org/10.3139/147.110683
39. Y. Ma, Y. Liu, J. Li, H. Zhang, and H. Yang, *Int. J. Mater. Res.*, **106**, No. 2: 151 (2015);
https://doi.org/10.3139/146.111158
40. H. Baker, *ASM Handbook Volume 3* (ASM International: Materials Park (OH): 1992) p. 281.
41. *Benxi Iron & Steel Co. Boron Steel*, 2. (Beijing: Metallurgical Industry Press: 1977) (in Chinese).
42. C. Guo and P.M. Kelly, *Mater. Sci. Eng. A*, **352**, Nos. 1–2: 40 (2003);
https://doi.org/10.1016/S0921-5093(02)00449-5
43. N. Filonenko and O. Galdina, *Phys. Chem. Solid State*, **17**, No. 2: 251 (2016);
https://doi.org/10.15330/pcss.17.2.251-255
44. O.K. von Goldbeck, *Iron-Binary Phase Diagramms* (Berlin–Heidelberg: Springer-Verlag: 1982);
https://doi.org/10.1007/978-3-662-08024-5_8
45. C. Kapfenberger, B. Albert, R. Pottgen, and H. Huppertz, *Zeitschrift fur Kristallographie-Crystalline Materials*, **221**, Nos. 5–7: 477 (2006);
https://doi.org/10.1524/zkri.2006.221.5-7.477
46. U. Sen, S. Sen, S. Koksal, and F. Yilmaz, *Mater. Des.*, **26**, No. 2: 175 (2005);
https://doi.org/10.1016/j.matdes.2004.05.015
47. S. Liu, X. Bian, J. Liu, J. Wang, M. Yu, Y. Yang, and R. Fan, *Intermetallics*, **94**: 186 (2018);
https://doi.org/10.1016/j.intermet.2017.12.027

48. J. Lentz, A. Ruttger, and W. Theisen, *Mater. Charact.*, **135**: 192 (2018); https://doi.org/10.1016/j.matchar.2017.11.012
49. D.W. Yi, J.D. Xing, H.G. Fu, Z.Y. Zhang, J. Chen, J.J. Zhang, J.H. Peng, and Y.P. Shi, *China Foundry*, **14**, No. 4: 272 (2017); https://doi.org/10.1007/s41230-017-6119-x
50. V.A. Barinov, V.A. Curin, S.I. Novikov, I.R. Shein, and V.T. Surikov, *Fiz. Met. Metalloved.*, **103**, No. 5: 497 (2007) (in Russian).
51. A. Gueddouh, B. Bentria, Y. Bourourou, and S. Maabed, *Materials Science-Poland*, **34**, No. 3: 503 (2016); https://doi.org/10.1515/msp-2016-0078
52. L.J. Xu, B.Y. Li, J.W. Li, G.S. Zhang, and S.Z. Wei, *Appl. Mech. Mater.*, **117–119**: 1406 (2011); https://doi.org/10.4028/www.scientific.net/AMM.117-119.1406
53. D. Yi, J. Xing, Z. Zhang, H. Fu, and C. Yang, *Tribol. Lett.*, **54**, No. 2: 107 (2014); https://doi.org/10.1007/s11249-014-0314-3
54. S. Ma and J. Zhang, *Rev. Adv. Mater. Sci.*, **44**, No. 1: 54 (2016);
55. K.D. Lakeland, E. Graham, and A. Heron, *Mechanical Properties and Microstructures of a Series of Fe–C–B Alloys* (15 Jan. 1992, Australia) (Brisbane: 1992).
56. J. Lentz, A. Rottger, and W. Theisen, *Acta Mater.*, **119**: 80 (2016); https://doi.org/10.1016/j.actamat.2016.08.009
57. O.V. Sukhova, *Phys. Chem. Solid State*, **21**, No. 2: 355 (2020); https://doi.org/10.15330/pcss.21.2.355-360
58. J. Lentz, A. Rottger, and W. Theisen, *Acta Mater.*, **99**: 119 (2015); https://doi.org/10.1016/j.actamat.2015.07.037
59. X. Chen and Y. Li, *Mater. Sci. Eng. A*, **528**, No. 2: 770 (2010); https://doi.org/10.1016/j.msea.2010.09.092
60. H. Fu, X. Song, Y. Lei, Z. Jiang, J. Yang, J. Wang, and J. Xing, *Met. Mater. Int.*, **15**, No. 3: 345 (2009); https://doi.org/10.1007/s12540-009-0345-8
61. C.Q. Guo, C.D. Wang, X.P. Liu, and P.M. Kelly, *China Foundry,* **5**, No. 1: 28 (2008).
62. X. Ren, H. Fu, J. Xing, and Y. Yi, *Mater. Sci. Eng. A*, **742**: 617 (2019); https://doi.org/10.1016/j.msea.2018.10.087
63. H. Fu, *Foundry*, **54**, No. 9: 859 (2005); https://doi.org/10.1007/s00101-005-0914-2
64. D. Yi, Z. Zhang, H. Fu, and C. Yang, *J. Mater. Eng. Perform.*, **23**: 673 (2014); https://doi.org/10.1007/s11665-013-0787-5
65. H. Fu, Q. Xiao, J. Kuang, Z. Jiang, and J. Xing, *Mater. Sci. Eng. A*, **466**, Nos. 1–2: 160 (2007); https://doi.org/10.1016/j.msea.2007.02.032
66. H. Fu and Z. Jiang, *Acta Metall. Sin.*, **42**, No. 5: 545 (2006) (in Chinese); https://doi.org/10.3321/j.issn:0412-1961.2006.05.020
67. Y.X. Li, Z.L. Liu, and X. Chen, *Int. J. Cast. Met. Res.*, **21**, Nos. 1–4: 67 (2008); https://doi.org/10.1179/136404608X361684
68. Z. Liu, Y. Li, X. Chen, and K. Hu, *Mater. Sci. Eng. A*, **486**, Nos. 1–2: 112 (2008); https://doi.org/10.1016/j.msea.2007.10.017
69. M. Yue, F. Han-guang, M. Shang-lin, and L. Yong-ping, *Materwiss Werksttech*, **45**, No. 10: 912 (2014); https://doi.org/10.1002/mawe.201400252
70. J. Zhang, J. Liu, H. Liao, M. Zeng, and S. Ma, *J. Mater. Res. Technol.*, **8**, No. 6: 6308 (2019); https://doi.org/10.1016/j.jmrt.2019.09.004

71. L. Feng and L. Zhenhua, *Mater. Res. Express*, **7**: 016551 (2020); https://doi.org/10.1088/2053-1591/ab65e9
72. H.G. Fu, Y.P. Lei, J.D. Xing, and L.M. Huang, *Ironmaking Steelmaking,* **35**, No. 5: 371 (2008); https://doi.org/10.1179/174328108X271484
73. H. Fu, D. Zou, Z. Jiang, J. Yang, J. Wang, and J. Xing, *Mater. Manuf. Processes*, **23**, No. 5: 469 (2008); https://doi.org/10.1080/10426910802103775
74. H.G. Fu, D.M. Fu, and J.D. Xing, *Mater. Manuf. Processes*, **23**, No. 2: 123 (2008); https://doi.org/10.1080/10426910701774353
75. H.G. Fu, *Zhuzao (Foundry),* **55**, No. 3: 292 (2006);
76. S. Ma, J. Xing, H. Fu, D. Yi, Y. Li, J. Zhang, B. Zhu, and Y. Gao, *Mater. Chem. Phys.*, **132**, Nos. 2–3: 977 (2012); https://doi.org/10.1016/j.matchemphys.2011.12.044
77. G. Liu, J. Xing, S. Ma, Y. He, H. Fu, Y. Gao, Y. Wang, and Y. Wang, *Metall. Mater. Trans. A*, **46**, No. 5: 1900 (2015); https://doi.org/10.1007/s11661-015-2820-9
78. X. Zhang, W. Chen, and H. Luo, *Tribol. Lett.*, **66**, No. 3: 1 (2018); https://doi.org/10.1007/s11249-018-1066-2
79. S. Ma, J. Xing, H. Fu, D. Yi, X. Zhi, and Y. Li, *Surf. Coat. Technol.*, **204**, No. 14: 2208 (2010); https://doi.org/10.1016/j.surfcoat.2009.12.010
80. S. Ma, J. Xing, Y. He, H. Fu, Y. Li, and G. Liu, *Acta Mater.*, **115**: 392 (2016); https://doi.org/10.1016/j.actamat.2016.06.016
81. Y. Wang J. Xing S. Ma G. Liu Y. He D. Yang, and Y. Bai, *Corros. Sci.*, **98**: 240 (2015); https://doi.org/10.1016/j.corsci.2015.05.039
82. S. Ma, J. Xing, D. Yi, H. Fu, J. Zhang, Y. Li, Z. Zhang, G. Liu, and B. Zhu, *Surf. Coat. Technol.*, **205**, Nos. 21–22: 4902 (2011); https://doi.org/10.1016/j.surfcoat.2011.04.101
83. S. Ma, J. Xing, H. Fu, Y. Gao, and J. Zhang, *Acta Mater.*, **60**, No. 3: 831 (2012); https://doi.org/10.1016/j.actamat.2011.11.004
84. Y. Jian, Z. Huang, J. Xing, X. Liu, L. Sun, B. Zheng, and Y. Wang, *Wear,* **362–363**: 68 (2016); https://doi.org/10.1016/j.wear.2016.04.029
85. L.I. Musen, F.U. Shaoli, X.U. Wandong, and Z.R.Y. Ruihuang, *Acta. Metall. Sin.*, **31**, No. 5: 201 (1995).
86. S. Ma, J. Zhang, and S. Ma, *Mater. Test.,* **58**, No. 2: 127 (2016); https://doi.org/10.3139/120.110834
87. D. Yi, J. Xing, S. Ma, H. Fu, W. Chen, Y. Li, J. Yan, J. Zhang, Z. Liu, and J. Zhu, *Tribol. Lett.*, **42**, No. 1: 67 (2011); https://doi.org/10.1007/s11249-011-9748-z
88. D. Yi, J. Xing, H. Fu, H. Fu, Z. Zhang, J. Zhang, C. Yang, S. Ma, and Y. Li, *Tribol. Lett.*, **58**, No. 2: 1 (2015); https://doi.org/10.1007/s11249-015-0501-x
89. J.-C. Kuang, H. Fu, C. Ye., Y.-Q. Liu, and Y.-P. Chen, *Journal of Sichuan University (Engineering Science Edition)*, **38**, No. 4: 105 (2006).
90. Z.L. Liu, X. Chen, Y.X. Li, and K.H. Hu, *J. Iron Steel Res. Int.*, **16**: 37 (2009); https://doi.org/10.1016/S1006-706X(09)60041-8
91. H. Fu, Q. Xiao, K. Qiang, J. Jiacai, X. Jiang, X. Zhiqiang, and J. Xing, *Mater. Sci. Eng.*, **466**: 160 (2007); https://doi.org/10.1016/j.msea.2007.02.032
92. Z. Liu, Y. Li, X. Chen, and K. Hu, *Foundry,* **56**, No. 4: 400 (2007).

93. X. Shi, Y. Jiang, and R. Zhou, *J. Iron Steel Res. Int.*, **23**, No. 11: 1226 (2016); https://doi.org/10.1016/S1006-706X(16)30180-7
94. J. Zhang, Y. Gao, J. Xing, S. Ma, D. Yi, L. Liu, and J. Yan, *J. Mater. Eng. Perform.*, **20**, No. 9: 1658 (2011); https://doi.org/10.1007/s11665-010-9809-8
95. L. He, Y. Liu, J. Li, and B. Li, *Mater. Des.*, **36**: 88 (2012); https://doi.org/10.1016/j.matdes.2011.10.043
96. J. Zhang, Y. Gao, J. Xing, X. Wei, S. Ma, and B. Che, *Tribol. Trans.*, **56**, No. 3: 461 (2013); https://doi.org/10.1080/10402004.2012.759304
97. D. Yi, J. Xing, S. Ma, H. Fu, W. Chen, Y. Li, J. Yan, J. Zhang, Z. Liu, and J. Zhu, *Tribol. Lett.*, **42**: 67 (2011); https://doi.org/10.1007/s11249-011-9748-z
98. S. Ma, J. Xing, G. Liu, D. Yi, H. Fu, J. Zhang, and Y. Li, *Mater. Sci. Eng. A*, **527**, No. 26: 6800 (2010); https://doi.org/10.1016/j.msea.2010.07.066
99. J. Lentz, A. Ruttger, F. Grozwendt, and W. Theisen, *Mater. Des.*, **156**: 113 (2018); https://doi.org/10.1016/j.matdes.2018.06.040
100. Y. Jian, Z. Huang, J. Xing, and B. Wang, *Mater. Charact.*, **110**: 138 (2015); https://doi.org/10.1016/j.matchar.2015.10.017
101. Z. Huang, J. Xing, and C. Guo, *Mater. Des.*, **31**, No. 6: 3084 (2010); https://doi.org/10.1016/j.matdes.2010.01.003
102. I. Goldfarb, W.D. Kaplan, S. Ariely, and M. Bamberger, *Philos. Mag. A*, **72**, No. 4: 963 (1995); https://doi.org/10.1080/01418619508239947
103. C.T. Zhou, J.D. Xing, B. Xiao, J. Feng, X.J. Xie, and Y.H. Chen, *Comput. Mater. Sci.*, **44**, No. 4: 1056 (2009); https://doi.org/10.1016/j.commatsci.2008.07.035
104. M.-M. Zhong, C. Huang, and C.-L. Tian, *Int. J. Mod. Phys. B*, **30**: 1650201 (2016); https://doi.org/10.1142/S0217979216502015
105. B. Wang, D.Y. Wang, Z. Cheng, X. Wang, and Y.X. Wang, *Chem. Phys. Chem.*, **14**: 1245 (2013); https://doi.org/10.1002/cphc.201201009
106. P. Christodoulou and N. Calos, *Mater. Sci. Eng. A*, **301**: 103 (2001); https://doi.org/10.1016/S0921-5093(00)01808-6
107. J. Lentz, A. Ruttger, and W. Theisen, *Steel Res. Int.*, **91**, No. 5: 103 (2019); https://doi.org/10.1002/srin.201900416
108. X. Wei, Z. Chen, J. Zhong, L. Wang, W. Yang, and Y. Wang, *Comput. Mater. Sci.*, **147**: 322 (2018); https://doi.org/10.1016/j.commatsci.2018.02.001
109. Y. Jian, Z. Huang, J. Xing, X. Guo, Y. Wang, and Z. Lv, *Tribol. Int.*, **103**: 243 (2016); https://doi.org/10.1016/j.triboint.2016.07.008
110. Y. Yi, J. Xing, Y. Lu, Y. Gao, H. Fu, L. Yu, M. Wan, and Q. Zheng, *Wear*, **408**: 160 (2018); https://doi.org/10.1016/j.wear.2018.05.014
111. Y. Yi, J. Xing, M. Wan, L. Yu, Y. Lu, and Y. Jian, *Mater. Sci. Eng. A*, **708**: 274 (2017); https://doi.org/10.1016/j.msea.2017.09.135

112. Y. Liu, B. Li, J. Li, L. He, S. Gao, and T.G. Nieh, *Mater. Lett.*, **64**, No. 11: 1299 (2010); https://doi.org/10.1016/j.matlet.2010.03.013
113. W. Hartono, S. Aso, S. Goto, and Y. Komatsu, *Int. J. Soc. Mater. Eng. Resour.*, **10**, No. 1: 99 (2002); https://doi.org/10.5188/ijsmer.10.99
114. S. Ma, J. Xing, S. Guo, Y. Bai, H. Fu, P. Lyu, Z. Huang, and W. Chen, *Mater. Chem. Phys.*, **199**: 356 (2017); https://doi.org/10.1016/j.matchemphys.2017.07.023
115. Z. Huang, J. Xing, and L. Lv, *Mater. Charact.*, **75**: 63 (2013); https://doi.org/10.1016/j.matchar.2012.09.007
116. X. Ren, L. Han, H. Fu, and J. Wang, *Materials,* **14**, No. 13: 3709 (2021); https://doi.org/10.3390/ma14133709
117. M. Frotscher, W. Klein, J. Bauer, C.-M. Fang, J.-F. Halet, A. Senyshyn, C. Baehtz, and B. Albert, *Zeitschrift für Anorganische und Allgemeine Chemie*, **633**, No. 15: 2626 (2007); https://doi.org/10.1002/zaac.200700376
118. H. Wang and T. Wang, *Mater. Lett.*, **285**: 129035 (2021); https://doi.org/10.1016/j.matlet.2020.129035
119. Z. Yu, H.G. Fu, Y.H. Jiang, Q.H. Cen, Y.P. Lei, R. Zhou, and H.X. Guo, *Materialwiss. Werkstofftech.*, **43**, No. 12: 1080 (2012); https://doi.org/10.1002/mawe.201200058
120. S. Ma, W. Pan, J. Xing, S. Guo, H. Fu, and P. Lyu, *Mater. Charact.*, **132**: 1 (2017); https://doi.org/10.1016/j.matchar.2017.08.001
121. X. Shi, Y. Jiang, Z. Li, and J. Hu, *Trans. Indian Inst. Met.*, **69**: 10 (2016); https://doi.org/10.1007/s12666-016-0839-2
122. Q. Cen and H. Fu, *Materialwiss. Werkstofftech.,* **44**, No. 7: 612 (2013); https://doi.org/10.1002/mawe.201300090
123. J. A. Jimenez, G. GonzalezDncel, and O. A. Ruano, *Adv. Mater.*, **7**, No. 2: 130 (1995); https://doi.org/10.1002/adma.19950070205
124. C. Xiang, L. Yanxiang, W. Zhisheng, Z. Huawei, and L. Yuan, *Rare Met. Mater. Eng.*, **47**, No. 3: 803 (2018).
125. V.G. Efremenko, K. Shimizu, A.P. Cheiliakh, T.V. Kozarevs'ka, Y.G. Chabak, H. Hara, and K. Kusumoto, *J. Frict. Wear*, **34**, No. 6: 466 (2013); https://doi.org/10.3103/S1068366613060068
126. A. Bedolla-Jacuinde, R. Correa, J. G. Quezada, and C. Maldonado, *Mater. Sci. Eng. A*, **398**, Nos. 1–2: 297 (2005); https://doi.org/10.1016/j.msea.2005.03.072
127. K. Kusumoto, K. Shimizu, X. Yaer, Y. Zhang, Y. Ota, and J. Ito, *Wear*, **376**: 22 (2017); https://doi.org/10.1016/j.wear.2017.01.096
128. J. Lu, J. Zhao, and L. Fenghua, *Metall. Mater. Trans. A*, 53: 1 (2022); https://doi.org/10.1007/s11661-022-06718-x
129. Y.F. Zhou, Y.L. Yang, D. Li, J. Yang, Y.W. Jiang, X.J. Ren, and Q.X. Yang, *Weld. J.*, **91**, No. 8: 229 (2012).
130. R.N. Jia, T.Q. Tu, K.H. Zheng, Z.B. Jiao, and Z.C. Luo, *Mater. Today Commun.*, **29**: 102906 (2021); https://doi.org/10.1016/j.mtcomm.2021.102906
131. Yu.G. Chabak and V.G. Efremenko, *Metallofiz. Noveishie Tekhnol.*, **34**: 1205 (2012).

132. Yu.G. Chabak, K. Shimizu, V.G. Efremenko, M.A. Golinskyi, K. Kusumoto, V.I. Zurnadzhy, and A.V. Efremenko, *Int. J. Miner. Metall. Mater.*, **29** No. 1: 78 (2022);
https://doi.org/10.1007/s12613-020-2135-8

Received 10.08.2022;
in final version, 13.10.2022

Ю.Г. Чабак[1,2], *В.І. Зурнаджи*[1], *М.А. Голинський*[1],
В.Г. Єфременко[1,2], *Н.П. Зайчук*[3], *І. Петришинець*[2], *С.П. Шимчук*[3]

[1] ДВНЗ «Приазовський державний технічний університет»,
вул. Університетська, 7; 87555 Маріуполь, Україна

[2] Інститут матеріалознавства Словацької академії наук,
вул. Ватсонова, 47; 04001 Кошице, Словаччина

[3] Луцький національний технічний університет,
вул. Львівська, 75; 43018 Луцьк, Україна

СУЧАСНІ ФУНКЦІОНАЛЬНІ МАТЕРІАЛИ ДЛЯ ЗНОСОСТІЙКОГО ЛИТТЯ: ВІД МУЛЬТИКОМПОНЕНТНИХ ЧАВУНІВ ДО ГІБРИДНИХ ВИСОКОБОРИСТИХ СТОПІВ

Розглядаються результати, одержані в останні два десятиріччя в галузі розробки функціональних трибологічних стопів, призначених для виготовлення литва, що працює в умовах інтенсивного абразивного, ерозійного й ерозійно-корозійного зношування. Аналізуються хімічний склад, мікроструктурні особливості, механічні та трибологічні властивості (а) багатокомпонентних чавунів, (б) стопів Fe–C–B з підвищеним (1–3,5 мас.%) вмістом Бору, а також (в) «гібридних» варіантів стопів, розроблених поєднанням різних підходів до леґування абразивностійких стопів. Робиться наголос на необхідності одержання гетерофазної структури, що складається із твердих сполук різних типів (карбідів, боридів, карбоборидів), розподілених у мартенситній матриці, зміцненій за рахунок вторинного твердіння. Такий структурний стан одержують одночасним введенням кількох сильних карбідоутворювальних елементів (Ti, W, Mo, V, Cr) у близьких пропорціях (за аналогією із високоентропійними стопами). Це приводить до конкуренції їх у фазоутворенні під час кристалізації, що забезпечує загальне дисперґування структурних елементів стопу. Показано перспективність часткової заміни Карбону на Бор у стопах на основі заліза, що уможливлює формування боридних і карбоборидних фаз із більш високою твердістю у порівнянні з карбідами. Це уможливлює досягнення високого рівня зносостійкости за відсутности (або низького вмісту) леґувальних елементів, що дає змогу істотно зменшити вартість литва. Проаналізовано вплив леґувальних елементів на фізико-механічні властивості боридних фаз, окреслено перспективи та представлено нові («гібридні») стопи, розроблені шляхом комбінування мультилеґування з підвищеним вмістом Бору. Описано основні технологічні підходи до оброблення борвмісних зносостійких стопів задля додаткового поліпшення їхніх механічних і трибологічних властивостей.

Ключові слова: багатокомпонентні чавуни, високоборисні чавуни, зносостійкість, мікроструктура, Бор, карбіди, бориди.